Modeling the relationship between $^{231}Pa/^{230}Th$ distribution in North Atlantic sediment and Atlantic meridional overturning circulation

Mark Siddall,[1,2] Thomas F. Stocker,[1] Gideon M. Henderson,[3] Fortunat Joos,[1] Martin Frank,[4] Neil R. Edwards,[5] Stefan P. Ritz,[1] and Simon A. Müller[1]

Received 11 August 2006; revised 13 November 2006; accepted 21 November 2006; published 19 May 2007.

[1] Down-core variations in North Atlantic $^{231}Pa_{xs}/^{230}Th_{xs}$ have been interpreted as changes in the strength of the Atlantic meridional overturning circulation (AMOC). This modeling study confirms that hypothetical changes in the AMOC would indeed be recorded as changes in the distribution of sedimentary $^{231}Pa_{xs}/^{230}Th_{xs}$. At different sites in the North Atlantic the changes in sedimentary $^{231}Pa/^{230}Th$ that we simulate are diverse and do not reflect a simple tendency for $^{231}Pa_{xs}/^{230}Th_{xs}$ to increase toward the production ratio (0.093) when the AMOC strength reduces but instead are moderated by the particle flux. In its collapsed or reduced state the AMOC does not remove ^{231}Pa from the North Atlantic: Instead, ^{231}Pa is scavenged to the North Atlantic sediment in areas of high particle flux. In this way the North Atlantic $^{231}Pa_{xs}/^{230}Th_{xs}$ during AMOC shutdown follows the same pattern as $^{231}Pa_{xs}/^{230}Th_{xs}$ in modern ocean basins with reduced rates of meridional overturning (i.e., Pacific or Indian oceans). We suggest that mapping the spatial distribution of $^{231}Pa_{xs}/^{230}Th_{xs}$ across several key points in the North Atlantic is an achievable and practical qualitative indicator of the AMOC strength in the short term. Our results indicate that additional North Atlantic sites where down-core observations of $^{231}Pa_{xs}/^{230}Th_{xs}$ would be useful coincide with locations which were maxima in the vertical particle flux during these periods. Reliable estimates of the North Atlantic mean $^{231}Pa_{xs}/^{230}Th_{xs}$ should remain a goal in the longer term. Our results hint at a possible "seesaw-like" behavior in $^{231}Pa/^{230}Th$ in the South Atlantic.

Citation: Siddall, M., T. F. Stocker, G. M. Henderson, F. Joos, M. Frank, N. R. Edwards, S. P. Ritz, and S. A. Müller (2007), Modeling the relationship between $^{231}Pa/^{230}Th$ distribution in North Atlantic sediment and Atlantic meridional overturning circulation, *Paleoceanography*, *22*, PA2214, doi:10.1029/2006PA001358.

1. Introduction

[2] ^{231}Pa and ^{230}Th are produced in the ocean by the α decay of ^{235}U and ^{234}U. The activity of U in the ocean is uniform [*Chen et al.*, 1986] so that ^{231}Pa and ^{230}Th are produced at a constant rate with a production activity ratio (β^{Pa}/β^{Th}) of 0.093 throughout the ocean. ^{231}Pa and ^{230}Th are removed from the open ocean by a process of reversible scavenging onto sinking particles [*Bacon and Anderson*, 1982; *Nozaki et al.*, 1987]. ^{231}Pa is scavenged from the water column less effectively than ^{230}Th and is transported over longer distances before deposition in the sediment [*Yu et al.*, 1996]. For this reason the sedimentary $^{231}Pa/^{230}Th$ reflects the combined effects of large-scale advection, diffusion and convection patterns in the ocean alongside vertical transfer linked to particulate fluxes [*McManus et al.*, 2004; *Marchal et al.*, 2000; *Siddall et al.*, 2005; *Thomas et al.*, 2006]. Sedimentary Pa/Th ratios may therefore provide information about the rate of past ocean circulation to complement information about the distribution of water masses recorded by tracers such as $\delta^{13}C$ and Cd/Ca. Such rate information is crucial to assessment of heat and carbon fluxes in the ocean, making $^{231}Pa/^{230}Th$ a potentially powerful tool to understand past climate change. The development of better understanding of the behavior of ^{231}Pa and ^{230}Th in the oceans is therefore an important goal.

[3] Sedimentary $^{231}Pa_{xs}/^{230}Th_{xs}$ has been extensively studied in the North Atlantic. (The xs subscript is used to indicate that the values represent excess ^{231}Pa and ^{230}Th activities which have been corrected for ^{231}Pa and ^{230}Th originating from U decay within the detrital particles of the sediments and thus only reflect the ^{231}Pa and ^{230}Th adsorbed from the water column.) The residence time for ^{231}Pa (100–200 years) is similar to the transit time of Atlantic water masses from the north to the Southern Ocean and thus a considerable amount of ^{231}Pa is exported from the North Atlantic to the Southern Ocean. In contrast, the residence time of ^{230}Th is of the order of several decades so that much less ^{230}Th is removed from the North Atlantic compared with ^{231}Pa. Therefore low $^{231}Pa_{xs}/^{230}Th_{xs}$ in the surface sediment of the North Atlantic is linked to the convection and advection of deep water masses in the North Atlantic (i.e., the Atlantic meridional overturning circulation (AMOC)). *Yu et al.* [1996] considered differences in the mean sedimentary $^{231}Pa_{xs}/^{230}Th_{xs}$ between the present day and the Last Glacial Maximum for the whole Atlantic to

[1]Climate and Environmental Physics, Physics Institute, University of Bern, Bern, Switzerland.
[2]Now at Lamont-Doherty Earth Observatory of Columbia University, Pallisades, New York, USA.
[3]Department of Earth Sciences, University of Oxford, Oxford, UK.
[4]IFM-GEOMAR, Leibniz Institute for Marine Sciences, University of Kiel, Kiel, Germany.
[5]Earth Sciences, Open University, Milton Keynes, UK.

0883-8305/07/2006PA001358$12.00

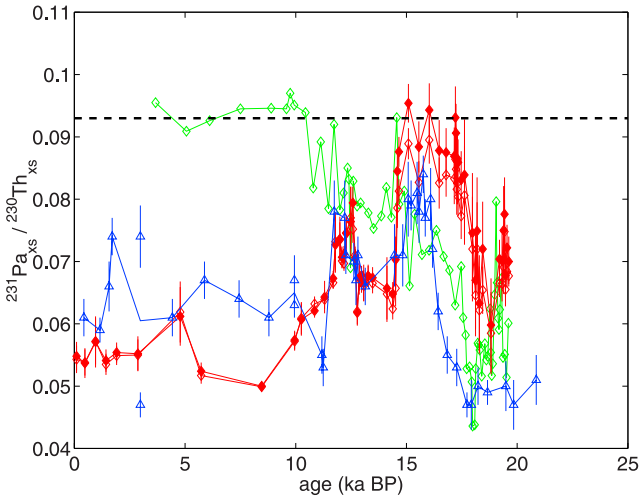

Figure 1. Down-core time series of $^{231}Pa_{xs}/^{230}Th_{xs}$ in cores from SiteW (33°42′N, 57°35′ W, 4550 m [*McManus et al.*, 2004]) (red), SiteE (37°46′N, 10°11′W, 3135 m [*Gherardi et al.*, 2005]) (blue), and SiteN (55°58′N, 09°36′W, 1709 m [*Hall et al.*, 2006]) (green). The core from SiteW was sampled twice using slightly different methods; see *McManus et al.* [2004] for details. The two records are demarcated using solid and open red markers. The black dashed line represents the production ratio (0.093).

suggest that there was little difference in the strength of the AMOC between the two periods. Using the Bern2.5D (zonally averaged) ocean model *Marchal et al.* [2000] showed that the mean sedimentary $^{231}Pa_{xs}/^{230}Th_{xs}$ for the North Atlantic was a more accurate measure of the AMOC than the mean sedimentary $^{231}Pa_{xs}/^{230}Th_{xs}$ for the whole Atlantic. The *Marchal et al.* [2000] study concluded that existing data were consistent with no glacial-to-recent change in AMOC strength, but do not rule out a reduction by up to 30%. The work of Marchal illustrated the usefulness of introducing ^{231}Pa and ^{230}Th into ocean models. Given the pronounced zonal differences in particle flux and ocean circulation across the North Atlantic their introduction into a model with a full three-dimensional configuration is a necessary step in improving our understanding of the dynamics of these nuclides in the ocean [*Siddall et al.*, 2005].

[4] Three sediment core records of $^{231}Pa_{xs}/^{230}Th_{xs}$ covering the last 20 ka have been published recently: *McManus et al.* [2004] described the $^{231}Pa_{xs}/^{230}Th_{xs}$ record from Atlantic core OCE 326-GGC5 on the western margin of the North Atlantic (33°42′N, 57°35′ W, 4550 m, from here on named SiteW): *Gherardi et al.* [2005] presented a record from the eastern North Atlantic (Core SU81-18, 37°46′N, 10°11′W, 3135 m, from here on named SiteE); and, *Hall et al.* [2006] described the record from a core in the far North Atlantic (DAPC2; 55°58′N, 09°37′W, 1709 m, from here on named SiteN).

[5] Importantly, at SiteW and SiteE, significant changes in the particle fluxes are not apparent in ^{230}Th-normalized sediment flux records so that changes in the sedimentary $^{231}Pa_{xs}/^{230}Th_{xs}$ are likely to be entirely due to changes in the AMOC. The $^{231}Pa_{xs}/^{230}Th_{xs}$ records from SiteW and SiteE are provided in Figure 1 and show broad similarities. There were pronounced increases in $^{231}Pa_{xs}/^{230}Th_{xs}$ at each site between 17 and 14 ka BP (i.e., broadly during the time of Heinrich event 1, H1) and smaller increases during the Younger Dryas (YD) [*McManus et al.*, 2004; *Gherardi et al.*, 2005]. *Gherardi et al.* [2005] note that the increase in $^{231}Pa_{xs}/^{230}Th_{xs}$ during H1 at SiteE lagged the changes in the SiteW record and is of shorter duration. The recovery of $^{231}Pa_{xs}/^{230}Th_{xs}$ following H1 and the YD was synchronous at both sites. The SiteN record presents a more complicated history of changes in particle flux. During the Holocene the $^{231}Pa_{xs}/^{230}Th_{xs}$ is at the production ratio. *Hall et al.* [2006] have suggested that this results from the high opal flux to the sediment at this site during the Holocene. During the glacial termination there are brief increases in $^{231}Pa_{xs}/^{230}Th_{xs}$ which are suggested to correspond with localized freshwater inputs close to SiteN [*Hall et al.*, 2006].

[6] Because the SiteW record approached the $^{231}Pa/^{230}Th$ production ratio during H1, it has been suggested that this record indicates a nearly total cessation of the AMOC during this period. The reasoning behind this suggestion is that if ^{231}Pa is not advected away from the North Atlantic it should be removed where it is produced and the sedimentary $^{231}Pa_{xs}/^{230}Th_{xs}$ should approach the $^{231}Pa/^{230}Th$ production ratio. However, this suggestion does not take into account the effects of horizontal eddy diffusion on the sedimentary $^{231}Pa_{xs}/^{230}Th_{xs}$, as will become clear in this paper.

[7] Diffusive processes drive a down-gradient transport of ^{231}Pa into areas of high particle flux, where the ^{231}Pa is removed. This leads to peaks in $^{231}Pa/^{230}Th$ in areas of high particle flux [*Lao et al.*, 1992; *Kumar et al.*, 1993], a process which has been named the "particle flux effect" [*Siddall et al.*, 2005] in order to avoid confusion with the term "boundary scavenging". In addition, different particle types scavenge varying proportions of the two isotopes: the "particle-type effect" [e.g., *Chase et al.*, 2002]. "Boundary scavenging" is the combined effect of this "particle-type effect" and the "particle flux effect" at ocean boundaries. Thus the distribution of particles plays an important role in the fractionation of $^{231}Pa/^{230}Th$ in the ocean [*Anderson et al.*, 1983; *Walter et al.*, 1997; *Chase et al.*, 2002; *Henderson and Anderson*, 2003; *Siddall et al.*, 2005; *Heinze et al.*, 2006]. (Note that *Siddall et al.* [2005] show that no "particle flux effect" is associated with the maximum in dust flux beneath the Saharan dust plume, indicating that dust is not a significant scavenger of ^{231}Pa). Indeed *Marchal et al.* [2000] found that surface sedimentary $^{231}Pa/^{230}Th$ ratios increase to levels well above the production ratio in areas with high particle flux during slowdowns or shutdowns of the AMOC in a zonally averaged model. Given the zonal differences in particle flux and ocean circulation across the North Atlantic these effects may be even more pronounced in a three-dimensional model.

[8] In this paper we attempt to improve our understanding of the effect of variations in the Atlantic meridional overturning circulation (AMOC) on the fractionation of ^{231}Pa

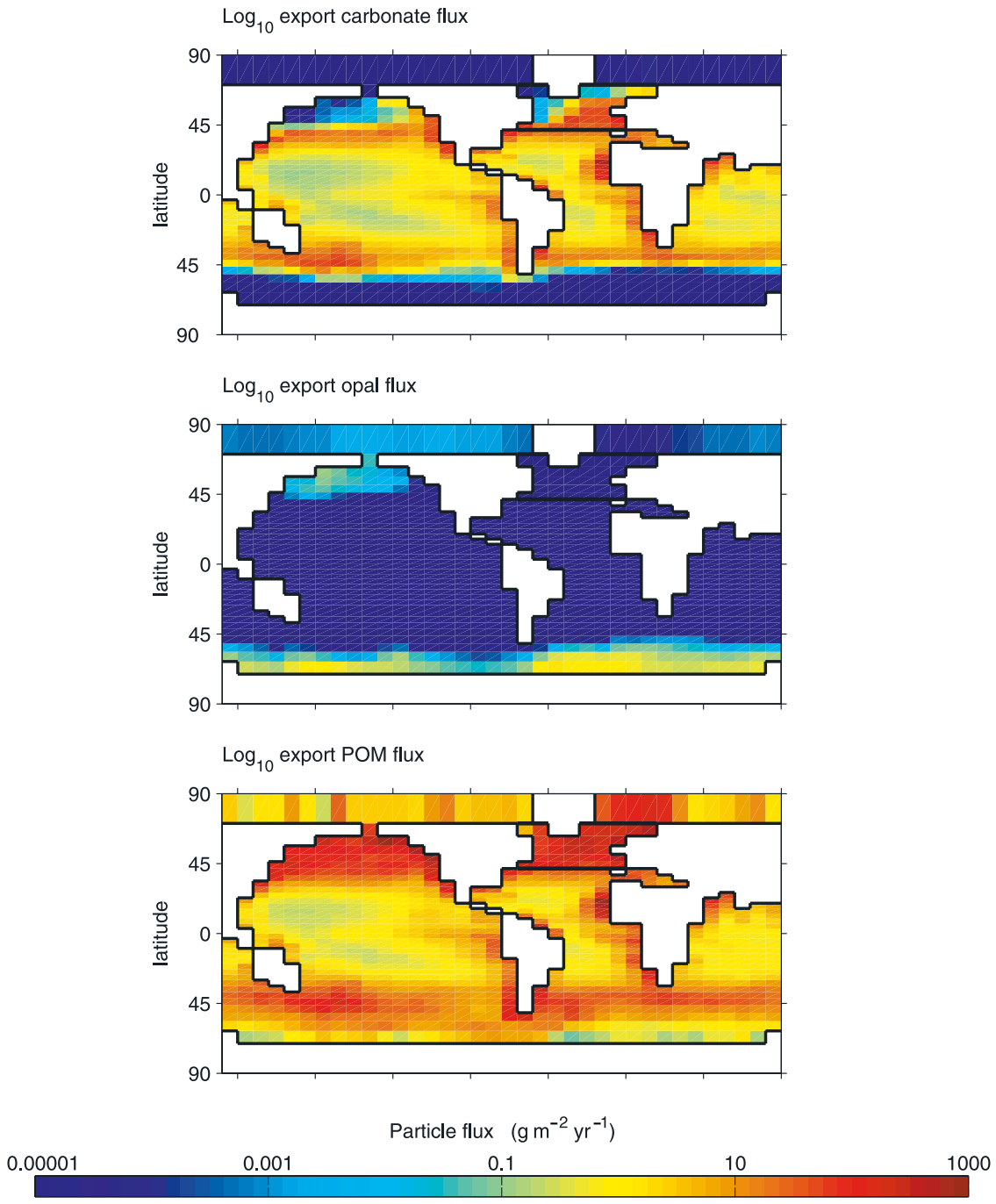

Figure 2. Particle fluxes used for the control run and most other runs. The freshwater forcing area used in the experiments as described in the text is between the thick black lines in the North Atlantic. This is also the area over which changes in the particle fluxes were applied (see section 3.3).

and ^{230}Th in the North Atlantic using the Bern3D model [*Müller et al.*, 2006].

2. Method

2.1. Bern3D Model

[9] The Bern3D model used in this work has been discussed in detail by *Müller et al.* [2006] and *Siddall et al.* [2005]. It transports tracers such as ^{231}Pa and ^{230}Th via advection, diffusion and convection processes within the Bern3D model [*Müller et al.*, 2006]. The Bern3D model is a computationally efficient ocean model of intermediate complexity based on the planetary geostrophic equations complemented by a linear drag term [*Edwards and Marsh*, 2005]. The model resolution is 36 by 36 grid squares of equal area across the globe in the horizontal plane with 32 depth levels. The Bern3D model simulates the large-scale circulation on seasonal and longer timescales reasonably well. The

Table 1. List of Equilibrium-Scavenging Coefficients (K Values) Used in the Text as Adapted From *Chase et al.* [2002] Following *Siddall et al.* [2005][a]

Variable	Symbol	Experiments
Equilibrium-scavenging coefficient	K_{ref}	10^7
^{230}Th scavenging by $CaCO_3$	K^{Th}_{car}	K_{ref}
^{230}Th scavenging by opal	K^{Th}_{opal}	$K_{ref}/20$
^{230}Th scavenging by POC	K^{Th}_{POC}	K_{ref}
^{230}Th scavenging by dust	K^{Th}_{dust}	0
^{231}Pa scavenging by $CaCO_3$	K^{Pa}_{car}	$K_{ref}/40$
^{231}Pa scavenging by opal	K^{Pa}_{opal}	$K_{ref}/6$
^{231}Pa scavenging by POC	K^{Pa}_{POC}	K_{ref}, $2 \times K_{ref}$, $K_{ref}/2$
^{231}Pa scavenging by dust	K^{Pa}_{dust}	0

[a]POC is particulate organic carbon.

AMOC in the model has a strength of 14 Sv, which is slightly weak compared to some other estimates, but within the range of observations (16 ± 3 Sv [*Ganachaud*, 2003] to 18.2 ± 2.5 Sv [*Talley et al.*, 2003]). We note especially that the previous work on this subject used a model with an unusually high AMOC of 24 Sv [*Marchal et al.*, 2000].

[10] Particle fields are prescribed using satellite-derived export productivity fields and appropriate dissolution profiles for each particle type. Particle dissolution in the model is discussed in detail by *Siddall et al.* [2005], and so here we provide a brief description: Dissolution of $CaCO_3$ with respect to depth is described by an exponential penetration profile; dissolution of particulate organic carbon (POC) with respect to depth is described by a power law; and dissolution of biogenic opal is described by a temperature (rather than depth) dependent dissolution scheme, which gives near vertical profiles at high latitude. Particles are subject to a uniform settling rate across all particle types: No distinction is made for particles of different size classes. *Siddall et al.* [2005] found that scavenging of ^{231}Pa and ^{230}Th by dust was not significant in controlling the broad pattern of ^{231}Pa and ^{230}Th distribution in the ocean so the dust flux is neglected for the purpose of the present study. Particle fields are shown in Figure 2. This approach has somewhat underrepresented the flux of opal in the northern North Atlantic and equatorial Pacific. This is not a significant problem because in these areas high particle fluxes compensates for the poorly represented ''particle-type effect'', explaining why the model adequately represents the modern sedimentary ^{231}Pa/^{230}Th distribution [*Siddall et al.*, 2005].

2.2. The ^{231}Pa and ^{230}Th Partition Coefficients

[11] A reversible scavenging model is applied to ^{231}Pa and ^{230}Th so that the process of adsorption onto falling particles and subsequent desorption at depth leads to an accumulation of ^{231}Pa and ^{230}Th with depth [*Bacon and Anderson*, 1982; *Roy-Barman et al.*, 1996]. Within such a scheme, adsorption/desorption takes place because of the sinking of particles to depths with different ^{231}Pa and ^{230}Th concentrations and because of particle dissolution. Nuclide adsorption/desorption processes linked to particle aggregation and disaggregation are not considered explicitly. As in the work of *Siddall et al.* [2005] an equilibrium-scavenging coefficient is used to describe the relationship between adsorbed and desorbed isotopes. This model assumes that ^{231}Pa and ^{230}Th in the water column are at equilibrium with falling particles.

[12] Such equilibrium-scavenging coefficients have often been used to describe the relationship between adsorbed and desorbed ^{231}Pa and ^{230}Th [*Henderson et al.*, 1999; *Chase et al.*, 2002; *Luo and Ku*, 1999, 2004a, 2004b; *Li*, 2005]. The dimensionless equilibrium-scavenging coefficient, K, is defined as the ratio between dissolved, A_d, and particle associated, A_p, activity:

$$K_p^i = \frac{A_p^i}{A_d^i C_p}, \tag{1}$$

where C_p is the dimensionless ratio of the particle mass per cubic meter to the density of the fluid and the activities are in units of dpm m^{-3}. The superscript i represents ^{231}Pa or ^{230}Th and the subscript p represents the particle type (POC, dust, $CaCO_3$ or opal). K values for separate particle types have proved difficult to observe directly [*Honeyman et al.*, 1988] and it is uncertain how readily laboratory assessment of their values [*Geibert and Usbeck*, 2004] can be extrapolated to the field. Modeling work has confirmed the observational assertion [*Chase et al.*, 2002] that the global ^{231}Pa/^{230}Th distribution in the ocean is largely controlled by the global distribution of the biogenic opal compared to $CaCO_3$ flux to the ocean sediments [*Marchal et al.*, 2000; *Siddall et al.*, 2005], the magnitude of the particle flux [*Bacon et al.*, 1976; *Anderson et al.*, 1983;

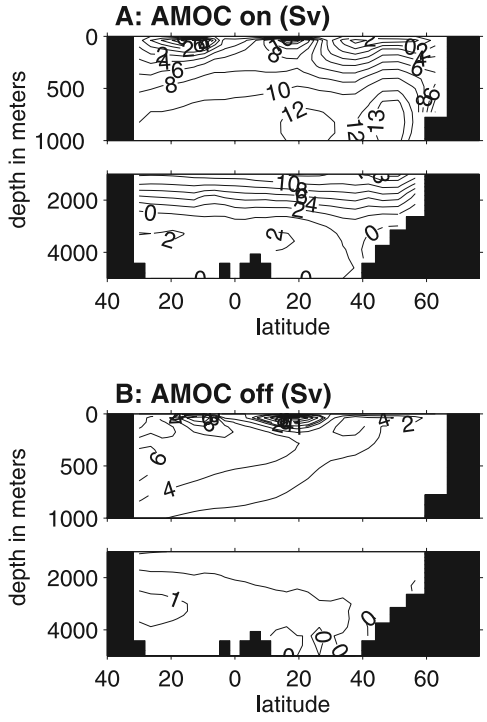

Figure 3. The annual mean stream function for the Atlantic meridional overturning circulation (AMOC) in the Bern3D ocean model for (a) the modern (AMOC-on) state ~14 Sv; and (b) the off state (~2 Sv).

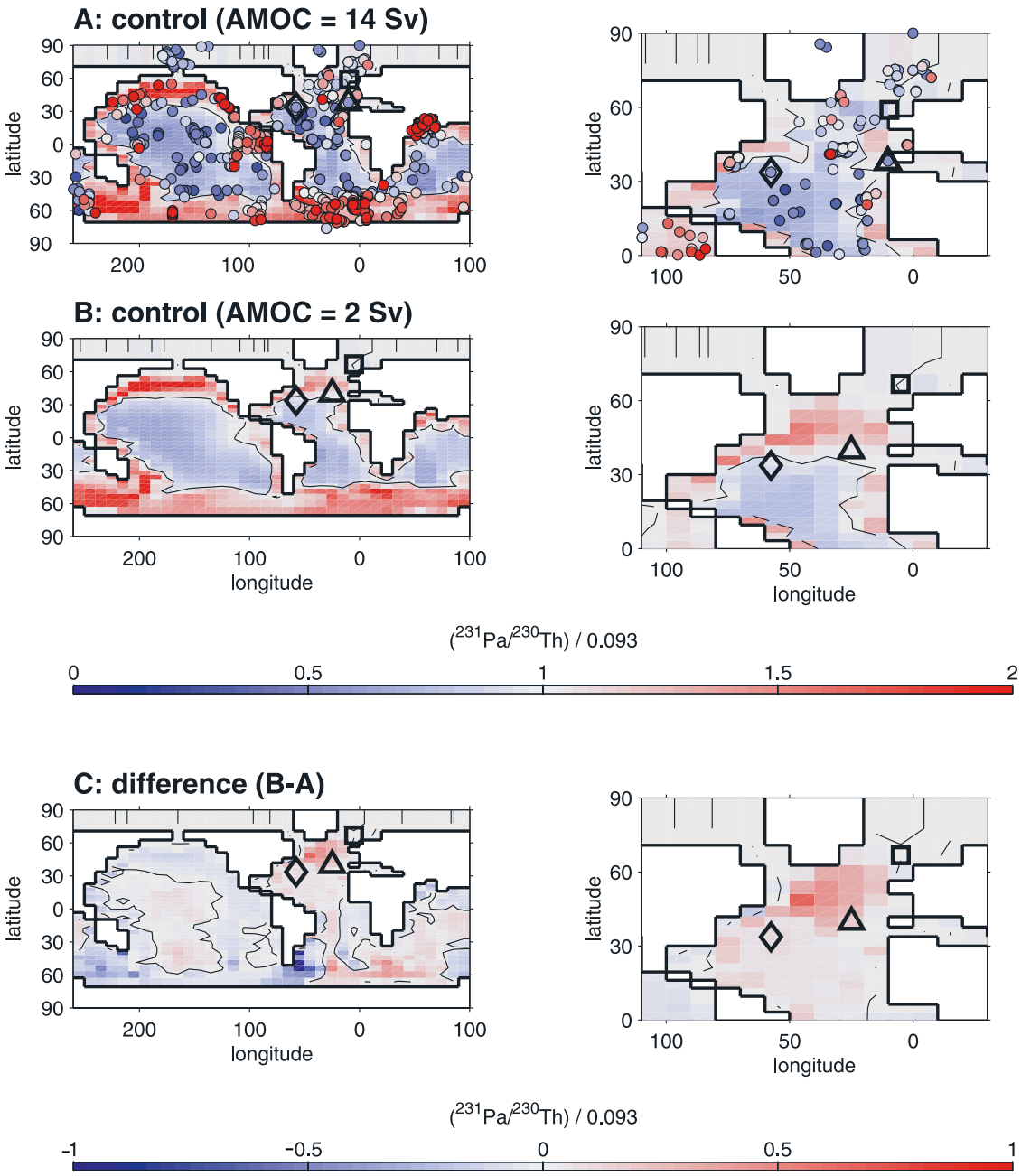

Figure 4. Model simulation of surface sedimentary $^{231}Pa_{xs}/^{230}Th_{xs}$ for (a) the control simulation of the present-day surface sedimentary $^{231}Pa_{xs}/^{230}Th_{xs}$ (AMOC-on, 14 Sv), as given by *Siddall et al.* [2005]. Observations are shown as colored circles. (b) Modeled surface sedimentary $^{231}Pa_{xs}/^{230}Th_{xs}$ for the AMOC-off state (2 Sv). (c) The difference in modeled surface sedimentary $^{231}Pa_{xs}/^{230}Th_{xs}$ between the AMOC-on and AMOC-off states. Actual sites are shown in Figure 4a and comparison sites are shown in Figures 4b and 4c: (diamond) SiteW; (triangle) SiteE; (square) SiteN. A complete list of the observational data shown here is given by *Siddall et al.* [2005].

Anderson et al., 1990] and deep ocean advection [*Marchal et al.*,2000; *Siddall et al.*, 2005].

[13] Values for equilibrium partition coefficients used in this study are given relative to a reference value which is approximately equivalent to the partition coefficient of ^{230}Th with respect to $CaCO_3$ ($K_{ref} = 1 \times 10^7$) [*Chase et al.*, 2002]. Values for equilibrium partition coefficients used in this paper are summarized in Table 1 and are identical to those used by *Siddall et al.* [2005].

[14] Boundary scavenging is the range of processes by which particle-reactive elements are preferentially removed to the sediment at ocean margins, including both high productivity and particle-type effects [*Bacon et al.*, 1976; *Anderson et al.*, 1983; *Anderson et al.*, 1990]: High

lithogenic flux from rivers/coastal erosion provides a primary source of additional particulate flux for scavenging and the supply of nutrients from rivers increases primary productivity, in turn also increasing the particulate flux available for scavenging close to the coasts. High-productivity upwelling zones near the coast are represented by the model but there is no representation of the input of lithogenic material at the coast. Boundary scavenging is effectively represented in the model only by the effect of higher productivity related to upwelling areas in grid boxes close to the coast. The potential effect of nepheloid layers on the ^{231}Pa and ^{230}Th is also not explicitly considered here other than that the sedimentary ^{231}Pa/^{230}Th is equilibrated with the water immediately above the sediment-water interface. In this way this work is directly parallel to that presented by *Thomas et al.* [2006] who considered a 1D model of ^{231}Pa/^{230}Th in the ocean for which equilibrium scavenging occurred at the sediment-water interface. Redissolution of ^{231}Pa and ^{230}Th from the surface sediment is not considered and is not thought to be significant [*François et al.*, 2007]. There has been some suggestion that particle size classes may scavenge differentially and that particles in smaller size classes cannot sink without undergoing aggregation. We do not account for this process explicitly here but we note that these particles may effectively be considered as part of the dissolved phase in our model. Taking these limitations into account we are attempting here to understand the broad spatial pattern of changes in ^{231}Pa/^{230}Th fractionation as a result of severe changes to the AMOC: We anticipate that our simplified model will be useful as a first step in understanding these changes. We note that the model we present is capable of representing the modern sedimentary ^{231}Pa/^{230}Th distribution [*Siddall et al.*, 2005] and so we feel justified in these assumptions.

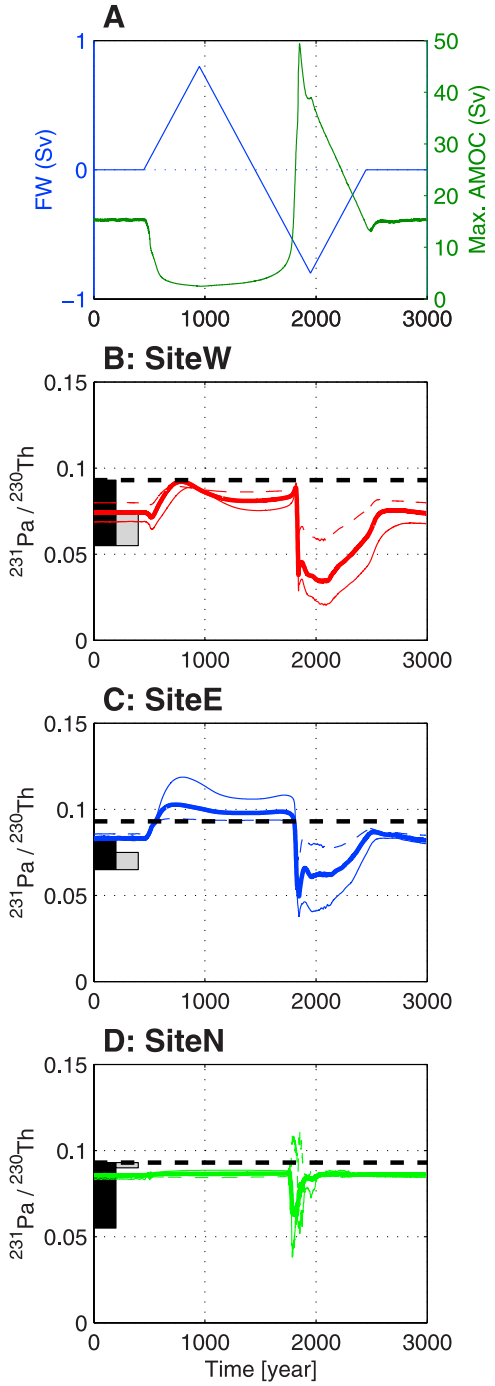

Figure 5. The evolution of overturning and sedimentary ^{231}Pa/^{230}Th for three sites during the reduced AMOC run. (a) Freshwater forcing (up to 8 Sv over 1000 years, left axis) was applied to the North Atlantic in the region shown in Figure 2. An identical, but negative, freshwater forcing was applied to force the recovery of the AMOC. The overturning collapses from 14 Sv to 2 Sv (right axis). Three cases were considered: the control (thick lines); scavenging of ^{231}Pa by particulate organic carbon (POC) halved (thin lines); and scavenging of ^{231}Pa by POC doubled (thin dashed lines). Figures 5b–5d show these cases at three sites: (b) SiteW (33°42′N, 57°35′ W, 4550 m [*McManus et al.*, 2004]); (c) SiteE (37°46′N, 10°11′W, 3135 m [*Gherardi et al.*, 2005]); and (d) SiteN (55°58.1′N, 09°36.75′W, 1709 m [*Hall et al.*, 2006]). Black bars represent the H1 to Holocene observed range in ^{231}Pa/^{230}Th and gray bars represent the Younger Dryas (YD) to Holocene observed range in ^{231}Pa/^{230}Th. The thick dashed line represents the ^{231}Pa/^{230}Th production ratio (0.093).

2.3. Control Run

[15] Here we consider the effect of a shutdown of the AMOC to a value of 2 Sv from the steady state value of 14 Sv (Figure 3). We maintain the same control spin up as given by *Siddall et al.* [2005] for purposes of comparison. Details of the equilibrium scavenging coefficients used for the control run and spin up can be found in Table 1. Figure 4a compares surface sedimentary ^{231}Pa and ^{230}Th from the control run of *Siddall et al.* [2005] with observations. The sources for the observations shown in all of the figures in this paper are listed by *Siddall et al.* [2005].

[16] A shutdown of the AMOC to a value of 2 Sv from the steady state value of 14 Sv (Figure 3) is achieved by adding freshwater to the North Atlantic between 45 and 70 °N. The zone of freshwater addition is shown between the black lines in Figure 2. The freshwater flux is increased linearly over

Table 2. A Compilation of Published Residence Time Estimates for ^{231}Pa and ^{230}Th From Observations and Models

Reference	Observations/Model	^{231}Pa Residence Time, yr	^{230}Th Residence Time, yr
This paper: control run	model	116	43
This paper: $K^{Pa}_{POC} = K_{ref}/2$	model	212	43
This paper: $K^{Pa}_{POC} = K_{ref} \times 2$	model	63	43
Henderson and Anderson [2003]	observations	130	20
Yu et al. [1996]	observations	200	30
Anderson et al. [1983]	observations	50–100	10–50

500 model years to a peak of 0.8 Sv and reduced again to 0 Sv over 500 years, provoking the collapse of the AMOC. The effect of shutdown on the AMOC is shown in Figure 5a. There is an almost total cessation of the AMOC throughout the water column. An identical but negative freshwater flux is used to restart the AMOC following the shutdown (Figure 5a).

[17] As discussed above, the Bern3D model does not fully resolve processes adjacent to lateral boundaries. Diffusive processes and boundary scavenging may be somewhat exaggerated at such sites and we consider it unwise to compare observations with our model within one grid square of the coast. Unfortunately SiteE and SiteN are within one grid space of the coast in our model and therefore we opt to compare SiteE and SiteN data with equivalent sites one grid space closer to the open ocean and away from spurious effects of the coast in our model. The alternative sites give similar results to the grid squares around them, except to the grid squares adjacent to the coast. In other words our results are not sensitive to our precise choice of site unless it is adjacent to the coast. The data comparison site depths are always equivalent to the depths of the observations.

3. Freshwater Forcing Experiments

3.1. Changes in $^{231}Pa/^{230}Th$ During a Collapse of the AMOC

[18] The effect of AMOC shutdown on sedimentary $^{231}Pa/^{230}Th$ is shown as a time series for the three sites in Figure 5, and for the whole North Atlantic during complete shutdown in Figure 4b. In this principal experiment the particle fluxes were kept constant at our estimated modern values, as shown in Figure 2 and described above. The equilibrium scavenging coefficients are as in the control experiments of *Siddall et al.* [2005] (Table 2). The ratios follow a similar pattern of variation at SiteW and SiteE, with a range comparable with those in the observations. This result lends support to the idea that variations in $^{231}Pa/^{230}Th$ at both sites might be controlled by changes in the AMOC.

[19] The limitations of the model are apparent by comparison with data: The observed lead of changes in $^{231}Pa_{xs}/^{230}Th_{xs}$ at SiteW versus SiteE is not simulated (Figure 5). We put these differences down to the relative simplicity of the model and the limitations of our current approach. For example SiteE is very close to the Portuguese coast and may be subject to effects not resolved by the model. Both *Gherardi et al.* [2005] and *Hall et al.* [2006] point out the possible effect of variations in the precise location and timing of freshwater input in the ocean during such events and these effects are not well resolved in this model. It is also possible that the precise depth at which the two cores are placed plays a role in that the deep water masses which bathe the two core sites may vary (SiteW is approximately 1400 m deeper than SiteE) and that the representation of water mass movement in the model is not adequate to resolve this effect [*Müller et al.*, 2006]. This may also explain the offset values for the simulation of modern conditions at SiteE. A more detailed study of this phasing relationship and the relationship of changes in the $^{231}Pa/^{230}Th$ with respect to depth is beyond the scope of this paper but should be addressed in a future work.

[20] The observed variation in $^{231}Pa_{xs}/^{230}Th_{xs}$ at SiteN is not well reproduced; there is little change in $^{231}Pa/^{230}Th$ at the site in the simulations. We note that our simulations are initiated from present-day conditions and not LGM conditions. Differences in atmospheric boundary conditions (i.e., the presence or lack of sea ice) and/or particle flux between the LGM and modern day may explain the discrepancies between the SiteN record and our simulations. Indeed, *Hall et al.* [2006] suggest that the production ratio $^{231}Pa/^{230}Th$ found in their core during the Holocene is linked to the high level of opal in this core during the Holocene. The effects of changing particle flux during freshwater events are considered in section 3.3.

[21] The most striking feature of the simulations is a pronounced maximum in the sedimentary $^{231}Pa/^{230}Th$ ratios in the northern North Atlantic during AMOC shutdown. Shutting down the AMOC forces the North Atlantic $^{231}Pa/^{230}Th$ system into a state similar to the North Pacific or North Indian oceans, which are governed primarily by horizontal eddy diffusion toward areas of high particle flux: i.e., the ''particle flux effect''. Comparing Figure 2 and Figures 4b and 4c reveals that indeed the maximum in surface sedimentary $^{231}Pa/^{230}Th$ in the northern North Atlantic during an AMOC shutdown coincides with the maximum in particle flux.

[22] Our results agree with the modeling study of *Asmus et al.* [1999] which shows that $^{231}Pa/^{230}Th$ in the Southern Ocean is likely insensitive to changes in the AMOC. However there is an interesting hint at a seesaw-like response [e.g., *Stocker and Johnsen*, 2003] in the reduced $^{231}Pa/^{230}Th$ ratios off the Atlantic coast of South America during the period of freshwater forcing. This is due to an increase in the deep western boundary current in this location as a result of the reduced circulation in the North Atlantic.

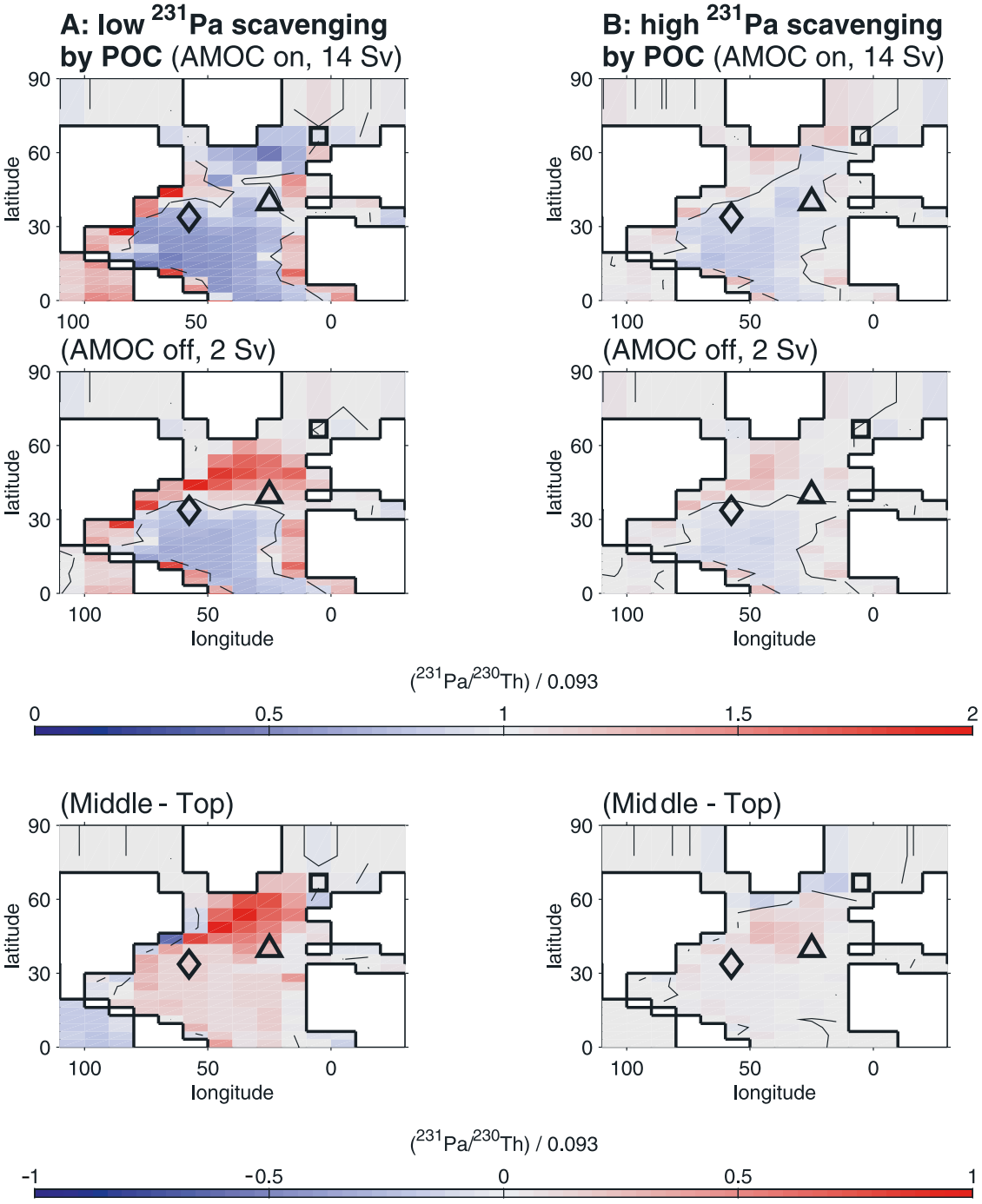

Figure 6. Model simulation of surface sedimentary $^{231}Pa_{xs}/^{230}Th_{xs}$ for the AMOC-on (14 Sv, top) and AMOC-off states (2 Sv, middle). Also shown is the difference in modeled surface sedimentary $^{231}Pa_{xs}/^{230}Th_{xs}$ between the AMOC-on and AMOC-off states (bottom). (diamond) SiteW; (triangle) SiteE; (square) SiteN. (a) The scavenging of ^{231}Pa by POC is halved ($K^{Pa}_{POC} = K_{ref}/2$). (b) The scavenging of ^{231}Pa by POC is doubled ($K^{Pa}_{POC} = K_{ref} \times 2$).

3.2. Sensitivity to Scavenging of ^{231}Pa by POC and the ^{231}Pa Residence Time

[23] An important uncertainty in the modeling of ^{231}Pa/^{230}Th is the significance of POC for ^{231}Pa/^{230}Th scavenging [*Dutay et al.*, 2006]. Here we consider the effect of varying $K^{Pa}{}_{POC}$ to assess the robustness of our conclusions to uncertainty in the role of POC scavenging. In the control simulation the scavenging of ^{231}Pa was set to the reference value (1×10^7). Here we consider uncertainty in the scavenging of ^{231}Pa by POC by varying the respective equilibrium-scavenging coefficient by a factor of 2 around the control reference equilibrium distribution coefficient.

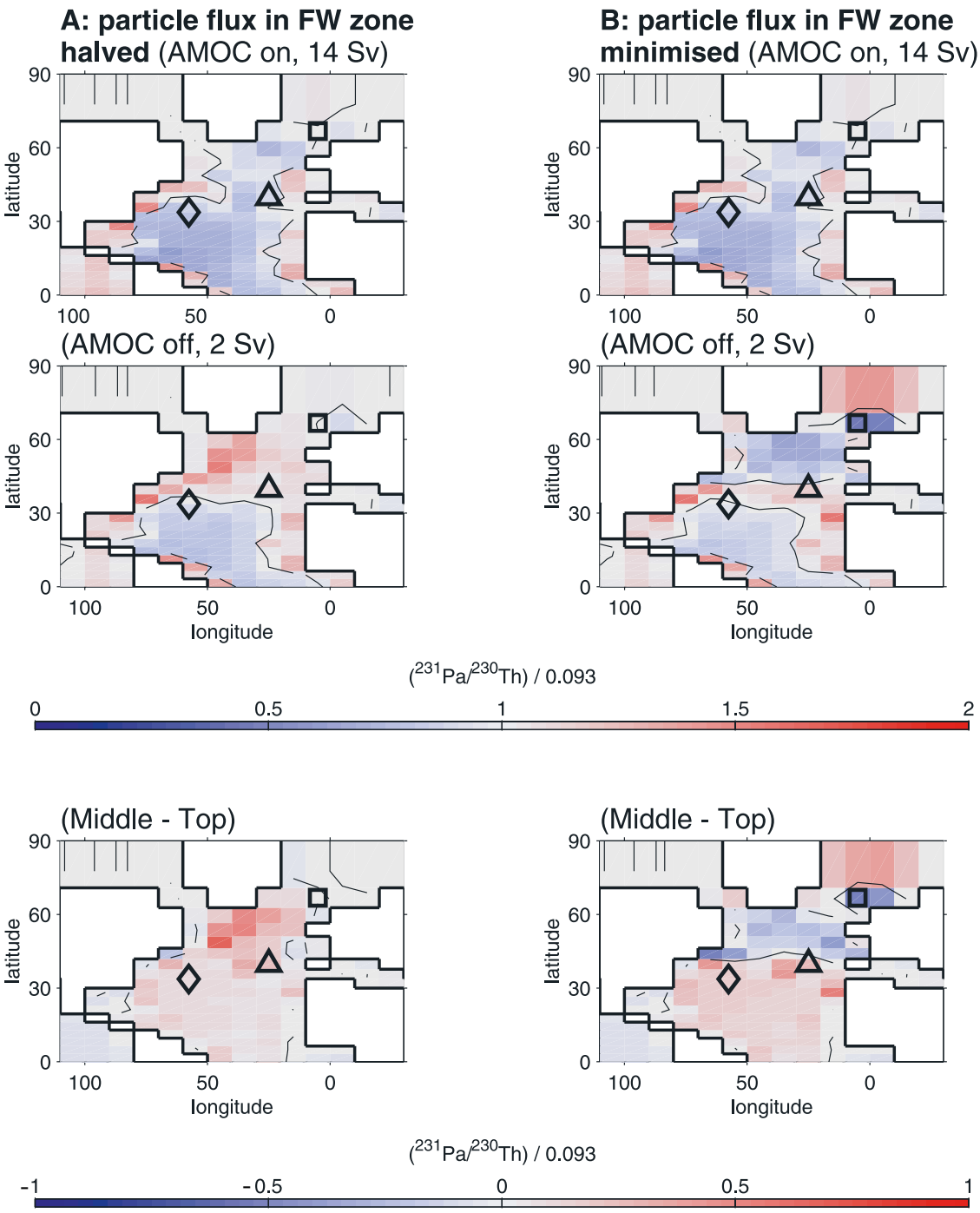

Figure 7. Model simulation of surface sedimentary $^{231}Pa_{xs}/^{230}Th_{xs}$ for the AMOC-on (14 Sv, top) and AMOC-off states (2 Sv, middle). Also shown is the difference in modeled surface sedimentary $^{231}Pa_{xs}/^{230}Th_{xs}$ between the AMOC-on and AMOC-off states (bottom). (diamond) SiteW; (triangle) SiteE; (square) SiteN. (a) Particle fluxes (opal, POC, $CaCO_3$) halved. (b) Particle fluxes fixed to a value typical of ocean gyres.

This allows us to consider the full range of published estimates for the residence times of ^{231}Pa (Table 2). The residence time of ^{230}Th in the model is low enough such that ^{230}Th is removed to the sediment before lateral transport in the ocean can have a strong effect. In this range changes by a factor of 2 to K^{Th}_{POC} do not alter the sedimentary $^{231}Pa/^{230}Th$ ratios substantially because the residence time of ^{230}Th remains considerably less than the time needed to achieve lateral transport of ^{230}Th by the ocean. Experiments varying K^{Th}_{POC} are not included here for reasons of brevity and for the fact that there is little to learn from them in this context.

[24] Figures 4, 5, and 6 show that the qualitative behavior of the model runs is very similar in all three cases ($K^{Pa}_{POC} = K_{ref}$, $K^{Pa}_{POC} = K_{ref}/2$, $K^{Pa}_{POC} = K_{ref} \times 2$), giving us confidence that we are describing robust features of the ^{231}Pa/^{230}Th system. Quantitatively there are variations of the order of 10 to 20 % in the ^{231}Pa/^{230}Th ratio as a result of uncertainty in the scavenging of ^{231}Pa by POC (Figure 5). During the period of collapse the most dramatic changes to the ^{231}Pa/^{230}Th ratios occur for the weakest POC scavenging (Figure 5). This is because the residence time of ^{231}Pa in the water column is greatest for runs with weak POC scavenging, facilitating both the strongest advection of ^{231}Pa when the AMOC is on and diffusion of ^{231}Pa into areas of high particle flux when the AMOC is off. Importantly the most striking feature of the simulations, a pronounced maximum in the sedimentary ^{231}Pa/^{230}Th ratios in the North Atlantic, is common to all three simulations (compare simulations in Figures 6 and 4).

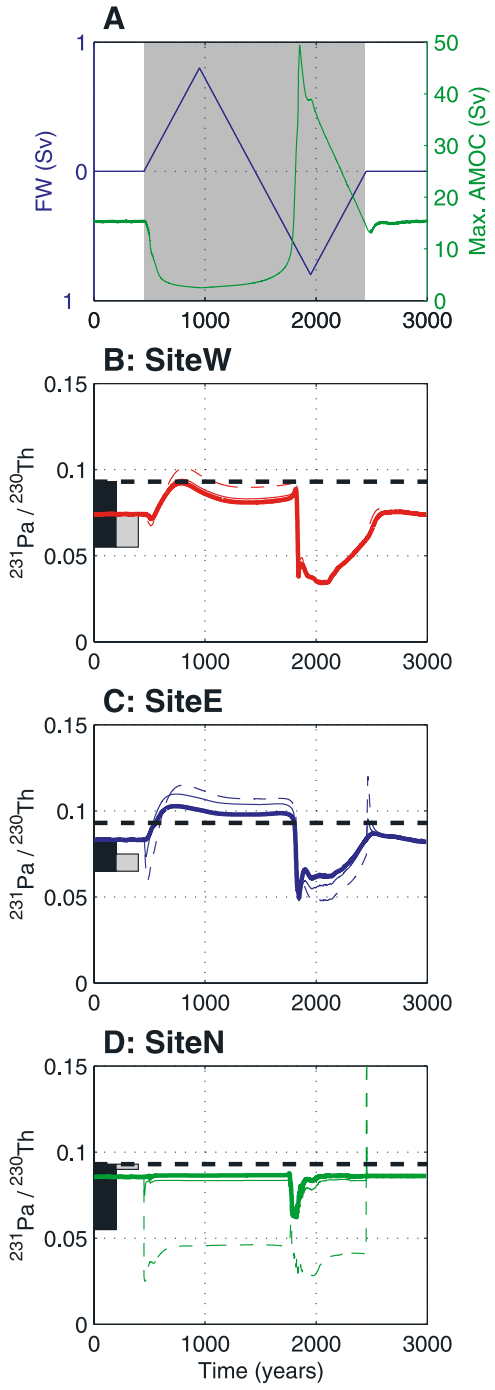

Figure 8. The evolution of overturning and sedimentary Pa/Th for three sites during the run with both reduced AMOC and altered particle fluxes. Three cases were considered: the control (thick lines); particle flux over the freshwater area halved (thin lines); and particle flux over the freshwater area set to a typical gyre value (thin dashed lines). (a) Freshwater forcing is identical to that in the reduced AMOC run (Figure 5). Particle fluxes were altered during the freshwater-forcing period illustrated by the gray box. Figures 8b–8d show these cases at three sites: (b) SiteW (33°42′N, 57°35′ W, 4550 m [*McManus et al.*, 2004]); (c) SiteE (37°46′N, 10°11′W, 3135 m [*Gherardi et al.*, 2005]); and (d) SiteN (55°58.1′N, 09°36.75′W, 1709 m [*Hall et al.*, 2006]). Black bars represent the H1 to Holocene observed range in ^{231}Pa/^{230}Th, and gray bars represent the YD to Holocene observed range in ^{231}Pa/^{230}Th. The thick dashed line represents the ^{231}Pa/^{230}Th production ratio (0.093).

3.3. Sensitivity to Changes in Particle Flux During a Collapse of the AMOC

[25] We have established that by keeping the particle flux constant during the experiments we observe the development of a pronounced ^{231}Pa/^{230}Th peak in the northern North Atlantic. Because this effect is due to the higher particle fluxes in the northern part of the North Atlantic compared to the southern part of the North Atlantic (Figure 2) it is important to take into account the possible effect of reductions in particle flux during a collapse of the AMOC. *Schmittner* [2005] shows the results of ensemble simulations of a coupled climate ecosystem model of intermediate complexity on the effect on biological productivity of a collapse of the AMOC resulting from surface freshwater forcing. This study found that the biological productivity in the northern North Atlantic is approximately halved during periods of freshwater forcing because of the nutrient limitation induced by the additional stratification which was caused by the imposition of a "freshwater lid" on the northern North Atlantic. On the basis of the results of *Schmittner* [2005] we consider the effect of halving the particle fluxes of $CaCO_3$, opal and POC in the zone of freshwater forcing (i.e., a scenario consistent with our experiments). Such a simple "cartoon" of changes in productivity neglects possible increases in particle flux in the equatorial Atlantic [e.g., *Hughen et al.*, 1996], decreases in the equatorial Pacific [e.g., *Bradtmiller et al.*, 2006] or in the subantarctic ocean [e.g., *Sachs and Anderson*, 2005]. We are not trying to generate an accurate map of ^{231}Pa/^{230}Th during a shutdown of the AMOC, rather this exercise is a means to begin to understand how our results might be sensitive to the covariation of particle fluxes with the AMOC strength. Changes to the particle flux are imple-

mented during the period of freshwater forcing. As an additional case of a possible extreme reduction in the particle flux beneath the freshwater forcing area we consider a simulation where $CaCO_3$, opal and POC fluxes are fixed to typical gyre values in order to consider particle fluxes from a region where present-day biological productivity is nutrient limited because of intense stratification.

[26] These model runs demonstrate that there is little difference from the control run as a result of halving the particle flux in the North Atlantic (compare Figures 4 and 7), which *Schmittner* [2005] found is the more realistic of the two scenarios during a freshwater forcing event. However, setting the particle flux to typical ocean gyre values leads to a minimum in $^{231}Pa/^{230}Th$ in the North Atlantic (Figures 7 and 8). This leads to an improved representation of the observed $^{231}Pa_{xs}/^{230}Th_{xs}$ at SiteN. Although such an extreme case may be unrealistic across much of the North Atlantic we speculate that this simulation may indicate the significance of reduced opal flux during the LGM and glacial termination as compared to the Holocene for the sedimentary $^{231}Pa_{xs}/^{230}Th_{xs}$ ratios: The relatively low opal flux during this period might sensitize SiteN to changes in circulation. Indeed, *Hall et al.* [2006] find coincident variation of $^{231}Pa_{xs}/^{230}Th_{xs}$ with the opal flux during the onset of the Holocene, supporting the idea that changes in particle flux have played an important role in setting sedimentary $^{231}Pa/^{230}Th$ in this region during the Holocene but that circulation effects play an important role during the LGM and the glacial termination. Given the limitations of the approach we take to the particle fluxes we do not want to overemphasize this interpretation but simply note that it is within the bounds of our sensitivity experiments.

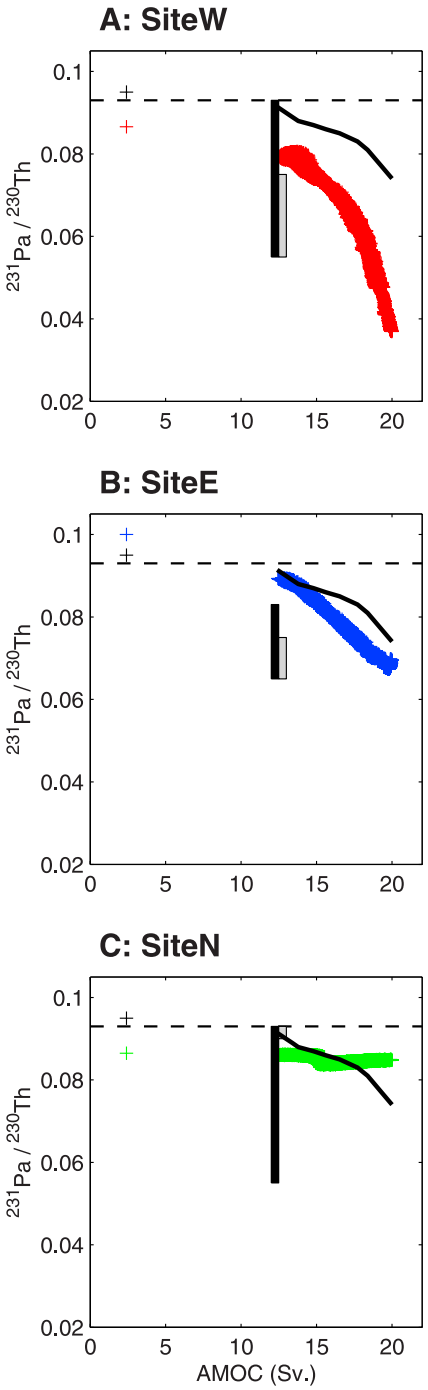

Figure 9. Plot of mean annual AMOC strength versus $^{231}Pa/^{230}Th$ at the three sites for three values of the scavenging of ^{231}Pa by POC. The control ($K^{Pa}_{POC} = K_{ref}$) is shown as darker areas. Figures 9a–9c show the data as broad bands, expressing the interannual variability in the AMOC in the Bern3D model. (a) SiteW (33°42′N, 57°35′W, 4550 m [*McManus et al.*, 2004]); (b) SiteE (37°46′N, 10°11′W, 3135 m [*Gherardi et al.*, 2005]); and (c) SiteN (55°58.1′N, 09°36.75′W, 1709 m [*Hall et al.*, 2006]). Black bars represent the H1 to Holocene observed range in $^{231}Pa/^{230}Th$, and gray bars represent the YD to Holocene observed range in $^{231}Pa/^{230}Th$. The thin dashed line represents the $^{231}Pa/^{230}Th$ production ratio (0.093). The thick black line is the North Atlantic mean (0 to 70°N) $^{231}Pa/^{230}Th$ ratio in the surface sediment for the control run. Colored crosses show modeled sedimentary $^{231}Pa/^{230}Th$ at each site during a shutdown. Black crosses show the North Atlantic mean $^{231}Pa/^{230}Th$ during a shutdown.

3.4. Slowdown Versus Shutdown During H1 and the Younger Dryas

[27] Here we address whether or not the available downcore $^{231}Pa_{xs}/^{230}Th_{xs}$ data may be explained by a slowdown of the AMOC during H1 and the Younger Dryas or whether a complete shutdown is required. The definition of slowdown versus shutdown remains model dependent. The Bern3D model does not support a stable AMOC strength between 12 Sv and 2 Sv (i.e., the AMOC strength collapses from 12 Sv to 2 Sv). Here we define a slowdown as a reduction from 14 Sv to 12 Sv and a shutdown as a collapse of the AMOC from 12 to 2 Sv. The Bern3D model has an AMOC which is relatively slow and we would also like to consider the effect of increasing the AMOC on the sedimentary $^{231}Pa/^{230}Th$ in the model.

[28] We consider this question for a realistic range of the AMOC strength by gradual varying the freshwater input to

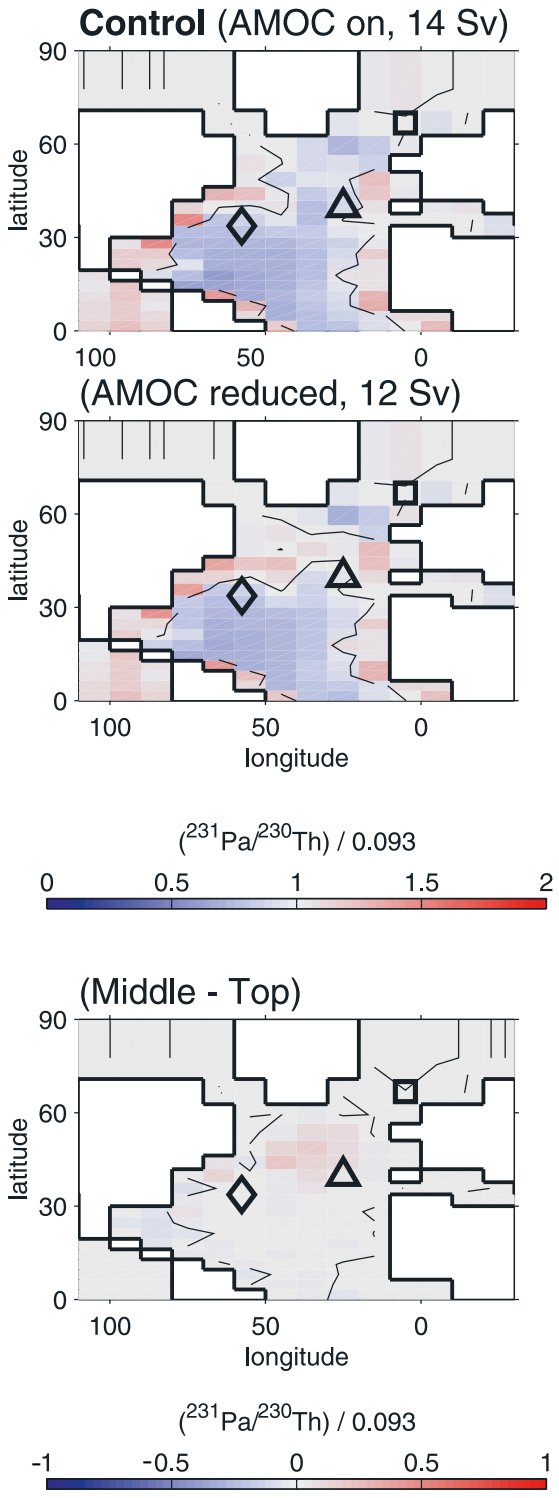

Figure 10. Model simulation of surface sedimentary $^{231}Pa_{xs}/^{230}Th_{xs}$ for the AMOC-on (14 Sv, top) and AMOC slowdown states (12 Sv, middle) for the control simulation. Also shown is the difference in modeled surface sedimentary $^{231}Pa_{xs}/^{230}Th_{xs}$ between the AMOC-on and slowdown states (bottom). (diamond) SiteW; (triangle) SiteE; (square) SiteN.

the North Atlantic up to the point where the AMOC collapses (at an overturning strength of 12 Sv). We then increase the AMOC strength up to 18 Sv by gradually applying a negative freshwater forcing over the North Atlantic. Such a negative freshwater forcing may be considered to represent an increased moisture flux from the Atlantic to the Pacific than is allowed for in the model. By varying the freshwater forcing slowly over thousands of years the model is always at quasi-equilibrium with the freshwater forcing and we can investigate the properties of the model during a slowdown, rather than a full collapse of the AMOC. The resulting plot of the AMOC strength versus modeled sedimentary ^{231}Pa/^{230}Th is shown in Figure 9. Figures 9a–9c show the data as broad bands, expressing the interannual variability in the AMOC in the Bern3D model with mixed boundary conditions.

[29] From Figure 9 it is clear that in our model a slowdown in the AMOC can explain the magnitude of the observed YD variability in $^{231}Pa_{xs}/^{230}Th_{xs}$. The available data are not conclusive on whether the AMOC shutdown or slowed down during the YD but we consider the fact that observed sedimentary $^{231}Pa_{xs}/^{230}Th_{xs}$ always remain below the ^{231}Pa/^{230}Th production ratio is more consistent with a slowdown than a shutdown.

[30] We may also use these results to assess any ambiguity in whether the observed sedimentary $^{231}Pa_{xs}/^{230}Th_{xs}$ ratios support a shutdown in the AMOC during H1 as has been suggested by several authors [*McManus et al.*, 2004; *Gherardi et al.*, 2005]. There is little ambiguity in the data or the model that H1 consisted of a more severe slowdown of longer duration than that during the YD. However, with the available $^{231}Pa_{xs}/^{230}Th_{xs}$ a shutdown of the AMOC cannot be confirmed: Comparing Figures 4 and 10 reveals that there is no difference between the slowdown and shutdown scenarios which is discernable at the core sites. The model results indicate that data from core sites in the high particle flux zone to the north of SiteW and to the northwest of SiteE (Figure 2) would help resolve this ambiguity in interpretation. If we consider that a halving of the particle flux is the most likely scenario during a freshwater event [*Schmittner*, 2005] then the model presented here suggests that $^{231}Pa_{xs}/^{230}Th_{xs}$ at these sites would show a pronounced peak during AMOC shutdown events while slowdown events may only cause a slight increase in $^{231}Pa_{xs}/^{230}Th_{xs}$ (compare Figures 10 and 4). One caveat to this suggestion is that this precise result depends on the exact location of the maximum particle flux. If the results of *Schmittner* [2005] are in error then our finding that the maximum in $^{231}Pa_{xs}/^{230}Th_{xs}$ would correspond with the maximum particle flux likely remains robust but the location of the maximum particle flux may differ. During AMOC shutdown North Atlantic ^{231}Pa/^{230}Th in the model shows similar characteristics to other ocean basins with reduced overturning circulation (Pacific, Indian Ocean) and this increases our confidence in this prediction (for the control simulation Figures 4a and 4b).

[31] We note that the model appears to capture some asymmetry between east and west in the North Atlantic: The variation of ^{231}Pa/^{230}Th with respect to the AMOC is

greater in the west than the east, in agreement with observations (Figure 1).

4. Further Discussion

[32] Here we have included experiments varying separately the particle flux and the scavenging of ^{231}Pa by POC. We have also carried out experiments covarying these parameters but no substantial new insight was gained beyond what is discussed here and so these experiments are not included.

[33] Under present-day conditions, ^{231}Pa is removed from the North Atlantic by advection and there is little variation in $^{231}Pa_{xs}/^{230}Th_{xs}$ across the basin (unlike other basins where deep advection is less significant). During a shutdown of the AMOC, however, ^{231}Pa is not removed by advection and the particle flux effect effectively concentrates ^{231}Pa in areas of high particle flux. The spatial distribution of $^{231}Pa/^{230}Th$ in the North Atlantic may therefore give a convincing fingerprint of changes in the strength of the AMOC. In order to identify this fingerprint cores should be taken from the northern North Atlantic. In this area the model predicts a spatial maximum in sedimentary $^{231}Pa/^{230}Th$ during a slowdown or a shutdown. This spatial maximum in sedimentary $^{231}Pa/^{230}Th$ coincides with the particle flux maximum in the northern North Atlantic (Figure 2). Cores taken from this region should show a more marked change during a shutdown than during a slowdown. An advantage of this approach is that we should be able to increase our confidence in the link between changes in the AMOC and H1 with a relatively small number of extra cores. Our method is limited by our assumed changes in the particle fluxes during changes to the AMOC. Should the particle fluxes vary during AMOC slowdowns or shutdowns in a fashion which is different to any of our scenarios the main conclusion that the maximum in $^{231}Pa/^{230}Th$ would coincide with the particle flux maximum is likely robust.

[34] Our results demonstrate that the spatial variability of sedimentary $^{231}Pa_{xs}/^{230}Th_{xs}$ in the North Atlantic is likely to increase during a slowdown or shutdown of the AMOC. Even under present day conditions (with relatively little basin-wide variability) the mean North Atlantic $^{231}Pa_{xs}/^{230}Th_{xs}$ ratio is sensitive to the effects of boundary scavenging, undersampling and the particle flux effect. It would take a substantial number of extra cores in order to generate an accurate value for the mean $^{231}Pa_{xs}/^{230}Th_{xs}$ during the glacial termination, LGM and Holocene. Our results indicate that an increased understanding of the spatial distribution of $^{231}Pa_{xs}/^{230}Th_{xs}$ in the North Atlantic sediment combined with studies of changes in particle flux in those cores might be a good way to proceed in the shorter term as adequate data to generate basin-wide mean values is generated. The northern sectors of the modern Pacific or Indian oceans may be the best analogies for understanding the sedimentary $^{231}Pa/^{230}Th$ system for the Atlantic during a period of slowdown or shutdown of the AMOC.

[35] Although it has not been a focus of the present study our results hint at a seesaw-like response during the period of freshwater forcing in the North Atlantic. The simulated reduction in $^{231}Pa/^{230}Th$ off the Atlantic coast of South America is due to the enhancement of bottom currents in this area during the period of reduced circulation in the North Atlantic.

[36] There are important limitations to our approach and fully quantitative interpretation of down-core changes in $^{231}Pa_{xs}/^{230}Th_{xs}$ remains elusive: There are significant gaps in our understanding of this proxy. Moreover these gaps in our understanding are nontrivial. Here we list a few: The interaction of the $^{231}Pa/^{230}Th$ system with processes of particle aggregation and disaggregation with subsequent variations in settling rate; the effect of particle size; and the effect of seasonal ''snow falls'' during periods of higher particle production [*Scholten et al.*, 2005] are all unknown and will need to be considered in future modeling and observational studies. Future work will need to consider changes in particle fluxes which are themselves generated by the model (as oppose to the imposed particle fields we apply here). Such model estimates will need to be well constrained by proxy estimates of these changes to the particle flux.

[37] **Acknowledgments.** Thanks to Roger François, Alex Thomas, and Nick McCave who provided unpublished ^{231}Pa and ^{230}Th data. Discussion with Ian Hall was useful in preparing this work. Jan Scholten provided very useful comments. Olivier Marchal and Jerry McManus have provided useful discussion. Funding was made available from the STOPFEN European Network research project (HRPN-CT-2002-00221). Support from the Swiss National Science Foundation and the University of Bern is acknowledged.

References

Anderson, R. F., M. P. Bacon, and P. G. Brewer (1983), Removal of ^{230}Th and ^{231}Pa from the open ocean, *Earth Planet. Sci. Lett.*, *62*, 7–23.

Anderson, R. F., Y. Lao, W. S. Broecker, S. E. Trumbore, H. J. Hofmann, and W. Wolfi (1990), Boundary scavenging in the Pacific Ocean: A comparison of ^{10}Be and ^{231}Pa, *Earth Planet. Sci. Lett.*, *96*, 287–304.

Asmus, T., M. Frank, C. Koschmieder, N. Frank, R. Gersonde, G. Kuhn, and A. Mangini (1999), Variations of biogenic particle flux in the southern Atlantic section of the Subantarctic Front during the late Quaternary: Evidence from sedimentary $^{231}Pa_{ex}$ and $^{230}Th_{ex}$, *Mar. Geol.*, *159*, 63–78.

Bacon, M. P., and R. F. Anderson (1982), Distribution of thorium isotopes between dissolved and particulate forms in the deep sea, *J. Geophys. Res.*, *87*, 2045–2056.

Bacon, M. P., D. W. Spencer, and P. G. Brewer (1976), $^{210}Pb/^{226}Ra$ and $^{210}Po/^{210}Pb$ disequilibria in seawater and suspended particulate matter, *Earth Planet. Sci. Lett.*, *32*, 277–296.

Bradtmiller, L. I., R. F. Anderson, M. Q. Fleisher, and L. H. Burckle (2006), Diatom productivity in the equatorial Pacific Ocean from the last glacial period to the present: A test of the silicic acid leakage hypothesis, *Paleoceanography*, *21*, PA4201, doi:10.1029/2006PA001282.

Chase, Z., R. F. Anderson, M. Q. Fleisher, and P. W. Kubik (2002), The influence of particle composition and particle flux on scavenging of Th, Pa and Be in the ocean, *Earth Planet. Sci. Lett.*, *204*, 215–219.

Chen, J. H., R. L. Edwards, and G. J. Wasserburg (1986), ^{238}U, ^{234}U and ^{232}Th in seawater, *Earth Planet. Sci. Lett.*, *80*, 241–251.

Dutay, J.-C., F. Lacan, M. Roy-Barman, and L. Bopp (2006), Simulation of the cycle of trace elements (Pa, Th) with the coupled ocean-biogeochemistry model ORCA-PISCES:

Implementation of a reversible scavenging model, *Geophys. Res. Abstr.*, *8*, 04337.

Edwards, N. R., and R. Marsh (2005), Uncertainties due to transport-parameter sensitivity in an efficient 3-D ocean-climate model, *Clim. Dyn.*, *24*, 415–433.

François, R., et al. (2007), Comment on "Do geochemical estimates of sediment focusing pass the sediment test in the equatorial Pacific?" by M. Lyle et al., *Paleoceanography*, *22*, PA1216, doi:10.1029/2005PA001235.

Ganachaud, A. (2003), Large-scale mass transports, water mass formation, and diffusivities estimated from World Ocean Circulation Experiment (WOCE) hydrographic data, *J. Geophys. Res.*, *108*(C7), 3213, doi:10.1029/2002JC001565.

Geibert, W., and R. Usbeck (2004), Adsorption of thorium and protactinium onto different particle types: Experimental findings, *Geochim. Cosmochim. Acta*, *68*, 1489–1501.

Gherardi, J.-M., L. Labeyrie, J. F. McManus, R. François, L. C. Skinner, and E. Cortijo (2005), Evidence from the northeastern Atlantic basin for variability in the rate of the meridional overturning circulation through the deglaciation, *Earth Planet. Sci Lett.*, *240*, 710–723.

Hall, I. R., S. B. Moran, R. Zahn, P. C. Knutz, C.-C. Shen, and R. L. Edwards (2006), Accelerated draw-down of meridional overturning in the late-glacial Atlantic triggered by transient pre-H event freshwater perturbation, *Geophys. Res. Lett.*, *33*, L16616, doi:10.1029/2006GL026239.

Heinze, C., M. Gehlen, and C. Land (2006), On the potential of ^{230}Th, ^{231}Pa, and ^{10}Be for marine rain ratio determinations: A modelling study, *Global Biogeochem. Cycles*, *20*, GB2018, doi:10.1029/2005GB002595.

Henderson, G. M., and R. F. Anderson (2003), The U-series toolbox for paleoceanography, *Rev. Mineral. Geochem.*, *52*, 493–531.

Henderson, G. M., C. Heinze, R. F. Anderson, and A. M. E. Winguth (1999), Global distribution of the ^{230}Th flux to ocean sediments constrained by GCM modelling, *Deep Sea Res., Part I*, *46*, 1861–1894.

Honeyman, B. D., L. S. Balistrieri, and J. W. Murray (1988), Oceanic trace metal scavenging: The importance of particle concentration, *Deep Sea Res., Part A*, *35*, 227–246.

Hughen, K. A., J. T. Overpeck, L. C. Peterson, and S. Trumbore (1996), Rapid climate changes in the tropical Atlantic region during the last deglaciation, *Nature*, *380*, 51–54.

Kumar, N., R. Gwiazda, R. F. Anderson, and P. N. Froelich (1993), $^{231}Pa/^{230}Th$ ratios in sediments as a proxy for past changes in Southern Ocean productivity, *Nature*, *362*, 45–48.

Lao, Y., R. F. Anderson, W. S. Broecker, S. E. Trumbore, H. J. Hofmann, and W. Wolfli (1992), Transport and burial rates of ^{10}Be and ^{231}Pa in the Pacific Ocean during the Holocene period, *Earth Planet. Sci. Lett.*, *113*, 173–189.

Li, Y.-H. (2005), Controversy over the relationship between major components of sediment-trap materials and the bulk distribution coefficients of ^{230}Th, ^{231}Pa and ^{10}Be, *Earth Planet. Sci. Lett.*, *233*, 1–7.

Luo, S., and T.-L. Ku (1999), Oceanic $^{231}Pa/^{230}Th$ ratio influenced by particle composition and remineralisation, *Earth Planet. Sci. Lett.*, *167*, 183–199.

Luo, S., and T.-L. Ku (2004a), On the importance of opal, carbonate, and lithogenic clays in scavenging and fractionating ^{230}Th, ^{231}Pa and ^{10}Be in the ocean, *Earth Planet. Sci. Lett.*, *220*, 201–211.

Luo, S., and T.-L. Ku (2004b), Reply to comment on "On the importance of opal, carbonate, and lithogenic clays in scavenging and fractionating ^{230}Th, ^{231}Pa and ^{10}Be in the ocean," *Earth Planet. Sci. Lett.*, *220*, 223–229.

Marchal, O., R. Francois, T. F. Stocker, and F. Joos (2000), Ocean thermohaline circulation and sedimentary $^{231}Pa/^{230}Th$ ratio, *Paleoceanography*, *15*, 625–641.

McManus, J. F., R. Francois, J.-M. Gherardi, L. D. Keigwin, and S. Brown-Leger (2004), Collapse and rapid resumption of Atlantic meridional circulation linked to deglacial climate changes, *Nature*, *428*, 834–837.

Müller, S. A., F. Joos, N. R. Edwards, and T. F. Stocker (2006), Water mass distribution and ventilation time scales in a cost-efficient, 3-dimensional ocean model, *J. Clim.*, *19*, 5479–5499.

Nozaki, Y., S. H. Yang, and M. Yamada (1987), Scavenging of thorium in the ocean, *J. Geophys. Res.*, *92*, 772–778.

Roy-Barman, M., J. H. Chen, and G. J. Wasserburg (1996), ^{230}Th-^{232}Th systematics in the central Pacific Ocean: The sources and fates of thorium, *Earth Planet. Sci. Lett.*, *139*, 351–363.

Sachs, J. P., and R. F. Anderson (2005), Increased productivity in the subantarctic ocean during Heinrich events, *Nature*, *434*, 1118–1121.

Schmittner, A. (2005), Decline of the marine ecosystem caused by a reduction in the Atlantic overturning circulation, *Nature*, *434*, 628–633.

Scholten, J. C., et al. (2005), Radionuclide fluxes in the Arabian Sea: The role of particle composition, *Earth Planet. Sci. Lett.*, *230*, 319–337.

Siddall, M., G. M. Henderson, N. R. Edwards, S. A. Müller, T. F. Stocker, F. Joos, and M. Frank (2005), $^{231}Pa/^{230}Th$ fractionation by ocean transport, biogenic particle flux and particle type, *Earth Planet. Sci. Lett.*, *237*, 137–155.

Stocker, T. F., and S. J. Johnsen (2003), A minimum thermodynamic model for the bipolar seesaw, *Paleoceanography*, *18*(4), 1087, doi:10.1029/2003PA000920.

Talley, L. D., J. L. Reid, and P. E. Robbins (2003), Data-based meridional overturning streamfunctions for the global ocean, *J. Clim.*, *16*, 3213–3226.

Thomas, A. L., G. M. Henderson, and L. F. Robinson (2006), Interpretation of the $^{231}Pa/^{230}Th$ paleocirculation proxy: New water-column measurements from the southwest Indian Ocean, *Earth Planet. Sci. Lett.*, *241*, 493–504.

Walter, H. J., M. M. Rutgers van der Loeff, and H. Hoeltzen (1997), Enhanced scavenging of ^{231}Pa relative to ^{230}Th in the South Atlantic south of the Polar Front: Implications for the use of the $^{231}Pa/^{230}Th$ ratio as a paleoproductivity proxy, *Earth Planet. Sci. Lett.*, *149*, 85–100.

Yu, E. F., R. Francois, and M. P. Bacon (1996), Similar rates of modern and last-glacial ocean thermohaline circulation inferred from radiochemical data, *Nature*, *379*, 689–694.

N. R. Edwards, Earth Sciences, Open University, P.O. Box 197, Milton Keynes MK7 6BJ, UK.

M. Frank, IFM-GEOMAR, Leibniz Institute for Marine Sciences, University of Kiel, Wischhofstrasse 1-3, D-24148 Kiel, Germany.

G. M. Henderson, Department of Earth Sciences, University of Oxford, Parks Road, Oxford OX1 3PR, UK.

F. Joos, S. A. Müller, S. P. Ritz, and T. F. Stocker, Climate and Environmental Physics, Physics Institute, University of Bern, Sidlerstrasse 5, CH-3012 Bern, Switzerland.

M. Siddall, Lamont-Doherty Earth Observatory of Columbia University, 61 Route 9W, Pallisades, NY 10964, USA. (siddall@ldeo.columbia.edu)